Chinese Chemical Letters 35 (2024) 109806

Contents lists available at ScienceDirect

Chinese Chemical Letters

journal homepage: www.elsevier.com/locate/cclet

Ambient electrosynthesis of urea from carbon dioxide and nitrate over Mo_2C nanosheet

Yue Zhang[a], Xiaoya Fan[b], Xun He[b], Tingyu Yan[a], Yongchao Yao[b], Dongdong Zheng[b], Jingxiang Zhao[a,*], Qinghai Cai[a], Qian Liu[c], Luming Li[c], Wei Chu[c], Shengjun Sun[d], Xuping Sun[b,d,*]

[a] College of Chemistry and Chemical Engineering, and Key Laboratory of Photonic and Electronic Bandgap Materials, Ministry of Education, Harbin Normal University, Harbin 150025, China
[b] Institute of Fundamental and Frontier Sciences, University of Electronic Science and Technology of China, Chengdu 610054, China
[c] Institute for Advanced Study, Chengdu University, Chengdu 610106, China
[d] College of Chemistry, Chemical Engineering and Materials Science, Shandong Normal University, Ji'nan 250014, China

ARTICLE INFO

Article history:
Received 15 January 2024
Revised 20 March 2024
Accepted 20 March 2024
Available online 22 March 2024

Keywords:
Mo_2C
Multiple active sites
C-N coupling
Electrocatalysis
Urea synthesis
Density functional theory calculation

ABSTRACT

Electrocatalytic synthesis of urea through C–N bond formation, converting carbon dioxide (CO_2) and nitrate (NO_3^-), presents a promising, less energy-intensive alternative to industrial urea production process. In this communication, we report the application of Mo_2C nanosheets-decorated carbon sheets (Mo_2C/C) as a highly efficient electrocatalyst for facilitating C–N coupling in ambient urea electrosynthesis. In CO_2-saturated 0.2 mol/L Na_2SO_4 solution containing 0.05 mol/L NO_3^-, the Mo_2C/C catalyst achieves an impressive urea yield of 579.13 μg h^{-1} mg^{-1} with high Faradaic efficiency of 44.80% at –0.5 V *versus* the reversible hydrogen electrode. Further theoretical calculations reveal that the multiple Mo active sites enhance the formation of $^*CO$ and $^*NH_2$ intermediates and facilitate their C–N coupling. This research propels the use of Mo_2C-based electrodes in electrocatalysis and accentuates the capabilities of binary metal-based catalysts in C–N coupling reactions.

© 2024 Published by Elsevier B.V. on behalf of Chinese Chemical Society and Institute of Materia Medica, Chinese Academy of Medical Sciences.

The extensive utilization of urea (nitrogen fertilizers, medical products, pesticides) has significantly propelled the growth of the urea industry [1,2]. Presently, industrial synthesis of urea involves two key thermochemical stages: (i) The conversion of nitrogen (N_2) and hydrogen (H_2) to ammonia (NH_3) at temperatures ranging from 450 °C to 600 °C and pressures between 100 bar and 250 bar; and (ii) the subsequent reaction of NH_3 with carbon dioxide (CO_2) to form urea at temperatures of 180–230 °C and pressures of 150–250 bar [3,4]. Despite being a prevalent technique for decades, the future of this technology faces challenges due to its stringent reaction conditions and the substantial requirement for liquid ammonia NH_3 [5]. In contrast, the emerging method of urea electrosynthesis, which involves coupling CO_2 with a nitrogen source under ambient conditions, offers an innovative pathway [6–11]. This pathway not only significantly reduces energy consumption but also plays a crucial role in addressing the energy crisis and mitigating global warming caused by excessive CO_2 emissions.

In the realm of urea electrosynthesis, the use of N_2 as a primary source for urea production has recently captured considerable attention [7,12-16]. The limited solubility of N_2 in water at ambient conditions and the high energy required to break its N≡N bond (941 kJ/mol), nevertheless, typically results in suboptimal performance [17–22]. Conversely, nitrate (NO_3^-), being water-soluble, is a more favorable nitrogen source for its relatively lower dissociation energy of the N=O bond (204 kJ/mol), which facilitates enhanced reaction kinetics for urea electrosynthesis [6,10,23-28]. In addition, the electrochemical reduction of NO_3^- is considered as an environmentally friendly method, particularly for its ability to remove the abundant yet harmful NO_3^- in groundwater [29,30]. At the mechanistic level, introducing NO_3^- as a nitrogen source involves the electrocatalytic reduction of CO_2 to $^*CO$ and NO_3^- to $^*NH_2$ on the catalyst's active surface, which followed by a non-electrocatalytic coupling that forms C–N bond for urea production [31]. Nonetheless, significant advancements in this field are currently hindered by the challenge of identifying efficient catalysts that can effectively facilitate the C–N bonding process.

Current research primarily center on indium (In)- [25,32-34], ruthenium (Ru)- [35,36], and copper (Cu)-based catalysts

* Corresponding authors.
E-mail addresses: zhaojingxiang@hrbnu.edu.cn (J. Zhao), xpsun@uestc.edu.cn (X. Sun).

https://doi.org/10.1016/j.cclet.2024.109806
1001-8417/© 2024 Published by Elsevier B.V. on behalf of Chinese Chemical Society and Institute of Materia Medica, Chinese Academy of Medical Sciences.

[9,26,27,37-40] for the electrosynthesis of urea. However, their on-scale applications are hindered by the high costs of In and Ru, and the susceptibility of Cu to corrosion during NO_3^- reduction [41–44]. In natural processes, the reduction of NO_3^- is accomplished *via* enzymatic cascades involving NO_3^- reductase with a molybdenum (Mo) cofactor, and Mo sites are also known to catalyze CO_2 reduction [45–47]. Recent study has also demonstrated the effectiveness of molybdenum oxide nanoclusters in urea electrolysis through the conversion of CO_2 and NO_3^- [48]. In comparison, 2D molybdenum carbide (Mo_2C) is emerging as a highly appealing material due to its higher conductivity and fully exposed Mo active sites [49–51]. Mo_2C has been reported to show activity in both NO_3^- and CO_2 reduction reaction [51–53]. It is thus anticipated that Mo_2C can significantly enhance the C–N coupling process required for efficient urea electrolysis.

Herein, we propose for the efficient urea electrosynthesis *via* the co-reduction of NO_3^- and CO_2 on Mo_2C nanosheets-decorated carbon sheets (Mo_2C/C). The as-prepared Mo_2C/C affords a high urea yield rate of 579.13 μg h^{-1} mg^{-1} and a high Faradaic efficiency (FE) of 44.80% at –0.5 V *versus* reversible hydrogen electrode (RHE). Furthermore, it demonstrates outstanding electrochemical stability, consistently performing well over a duration of 12 h and through 8 successive cycles. Additionally, we employed density functional theory (DFT) calculations to delve deeper into the underlying mechanisms of the urea electrosynthesis process.

The X-ray diffraction (XRD) pattern of Mo_2C/C, as shown in Fig. 1a, exhibits distinct diffraction peaks at approximately 34.53°, 38.05°, 35.59°, 52.31°, 61.87°, 69.77°, 72.83°, 74.99° and 75.99°. These peaks closely align with those of standard Mo_2C (JCPDS No. 03–065–8766) [52,54]. Additionally, a broadened diffraction peak at around 21.6° is attributed to carbon [55], originating from the pyrolysis of glucose. Scanning electron microscopy (SEM) image (Fig. 1b) reveals interconnected, relatively smooth carbon sheets. Transmission electron microscopy (TEM) images (Figs. 1c and d) depict densely packed nanosheets on the surfaces of carbon sheet. In Fig. 1e, the high-resolution TEM (HRTEM) image of Mo_2C/C is presented. The selected area electron diffraction (SAED) patterns and line scan of the HRTEM image, indicated by red boxes 1 and 2 in Fig. 1f and Fig. S1 (Supporting information) from Fig. 1e, confirm the good crystallinity of Mo_2C, featuring a lattice spacing of 0.256 nm, which corresponds to the (100) plane of Mo_2C. Elemental distribution analysis using high-angle annular. High-angle annular dark field scanning TEM (HAADF-STEM) and corresponding elemental imaging in Fig. 1g reveal a homogeneous distribution of Mo and C atoms across the structure, indicating that the sheet-like nanoparticles are composed of Mo_2C uniformly distributed within the carbon sheet. Subsequent X-ray photoelectron spectroscopy (XPS) analysis of Mo_2C/C provide insights into the surface electronic states. The Mo 3d spectra (Fig. 1h) show peaks at 228.9 and 231.98 eV, corresponding to the binding energies of Mo^{2+}, indicative of Mo_2C. Other doublets observed at 229.5/232.7 and 232.6/235.8 eV can be attributed to oxidized molybdenum phases Mo^{4+} and Mo^{6+}, respectively, likely due to surface oxidation [56,57]. The C 1s spectra (Fig. 1i) consist of three subpeaks at 284.8, 285.6, and 288.8 eV, which are assigned to Mo-C, C–C, and O=C–O bonds, respectively [55,58,59].

The intrinsic CO_2 reduction reaction (CO_2RR) and NO_3^- reduction reaction (NO_3RR) performance of Mo_2C/C were initially evaluated in an H-type electrochemical cell. The linear sweep voltammetry (LSV) curve in CO_2-saturated 0.2 mol/L Na_2SO_4 (Fig. 2a) ex-

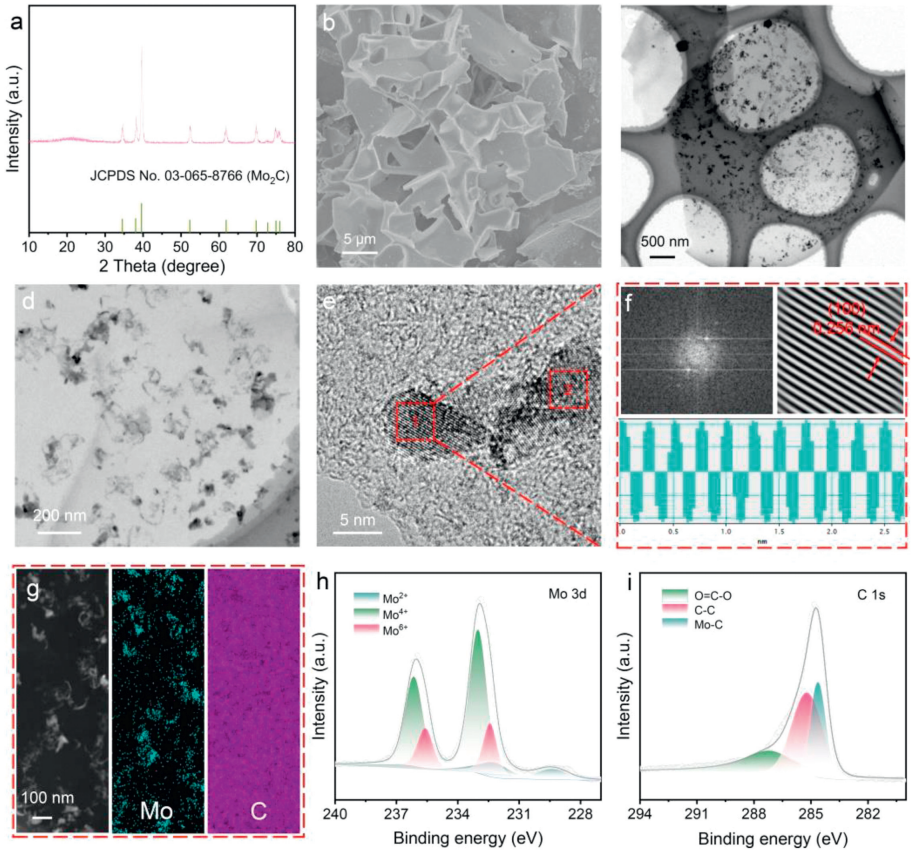

Fig. 1. (a) XRD pattern of Mo_2C/C. (b) SEM image of Mo_2C/C. (c) Low and (d) high magnification TEM images of Mo_2C/C. (e) High-resolution TEM image of Mo_2C/C. (f) SAED pattern and line scan and of the HRTEM image indicated by the red box 1 in (e). (g) HAADF-STEM and its corresponding mapping images of Mo_2C/C. XPS spectra of Mo_2C/C in the (h) Mo 3d, (i) C 1s regions.

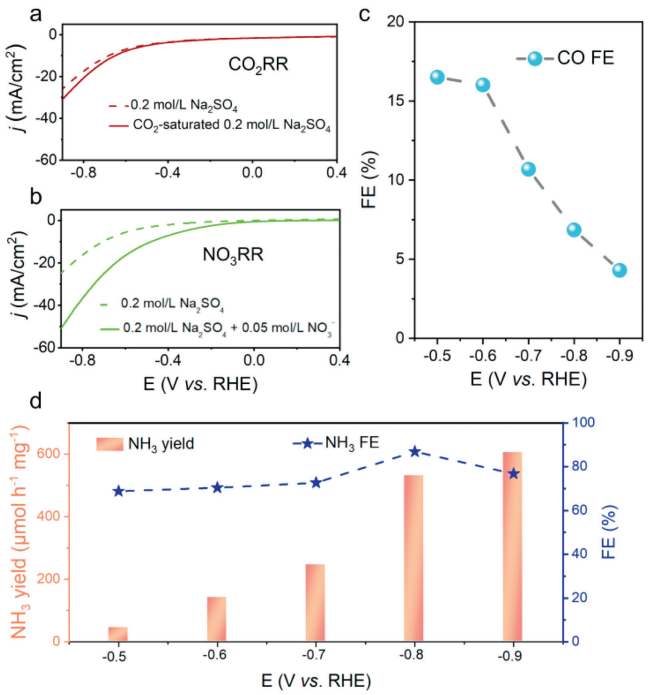

Fig. 2. (a) LSV curves of Mo_2C/C in 0.2 mol/L Na_2SO_4 with and without saturated CO_2, respectively. (b) LSV curves of Mo_2C/C in 0.2 mol/L Na_2SO_4 with and without 0.05 mol/L NO_3^-, respectively. (c) FEs of CO in CO_2RR process at various potentials on Mo_2C/C. (d) NH_3 yields and FEs on Mo_2C/C for NO_3RR in 0.2 mol/L Na_2SO_4 + 0.05 mol/L NO_3^- with various applied potentials.

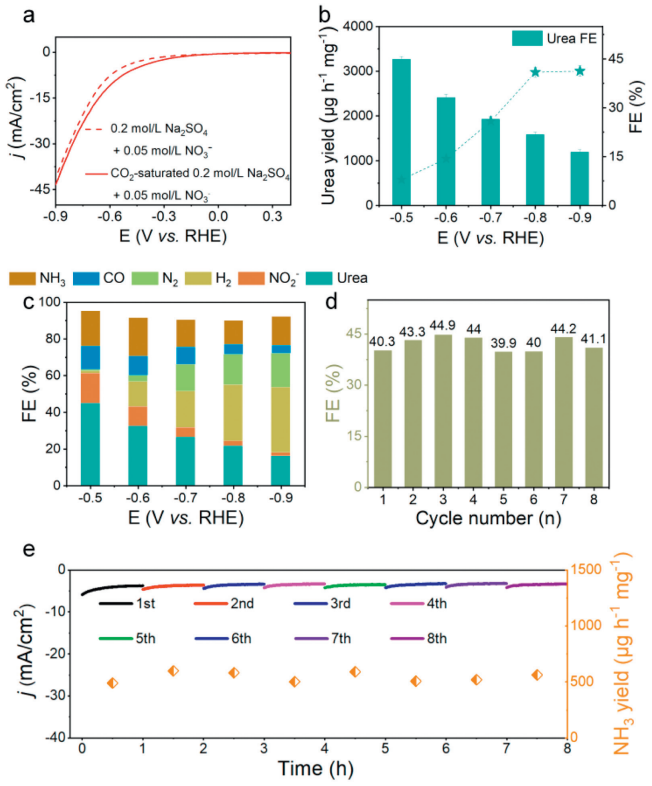

Fig. 3. (a) LSV curves of Mo_2C/C in Ar- and CO_2-saturated 0.2 mol/L Na_2SO_4 + 0.05 mol/L NO_3^-. (b) Urea yields and FEs of Mo_2C/C at different potentials. (c) FEs of NH_3, CO, N_2, H_2, NO_2^- and urea on Mo_2C/C at different potentials during the electrosynthesis of urea. (d) Urea FEs at −0.5 V during consecutive recycling test. (e) Urea yields and chronoamperometry curves during consecutive recycling test.

hibited a higher current density compared to that in pure 0.2 mol/L Na_2SO_4, indicating significant CO_2RR activity. Similarly, an obviously increase in current density was observed in 0.2 mol/L Na_2SO_4 containing 0.05 mol/L NO_3^-, demonstrating effective NO_3RR (Fig. 2b). Based on these LSV curves, the potential window from −0.5 V to −0.9 V was selected for subsequent CO_2RR and NO_3RR experiments, respectively. Mo_2C/C displayed commendable CO_2RR capacity for CO generation (Fig. 2c, Figs. S2 and S3 in Supporting information). The production of NH_3 was quantified using the indophenol blue method, with the corresponding calibration curve presented in Fig. S4 (Supporting information). Mo_2C/C also showed notable NO_3RR efficiency in generating NH_3 (Fig. 2d, Figs. S5 and S6 in Supporting information). In essence, the promising electrocatalytic performance of Mo_2C/C in both CO_2RR and NO_3RR underscores its potential for efficient electrocatalytic urea synthesis.

In the process of urea electrosynthesis, CO_2 was continuously bubbled into a solution of 0.2 mol/L Na_2SO_4 containing 0.05 mol/L NO_3^-. Initially, the potential performance was assessed using LSV curves (Fig. 3a). The presence of CO_2 elicited a current response, suggesting the potential occurrence of electrocatalytic C–N bonding crucial for urea synthesis. Subsequent chronoamperometry experiments were conducted to further confirm urea production (Fig. S7 in Supporting information). Urea detection was performed using the urease decomposition method, with corresponding UV–vis absorption spectra shown in Fig. S8 (Supporting information). And calculated urea yields and FEs at various potentials are presented in Fig. 3b. The UV–vis spectrum indicates a prominent absorbance at 655 nm at −0.9 V, corresponding to a urea yield of 3004.70 μg h^{-1} mg^{-1}. A high FE of 44.80% was recorded at −0.5 V, surpassing previously most of the reported urea electrosynthesis catalysts (Table S1 in Supporting information). Comprehensive evaluation of urea electrosynthesis also involved quantitative detection of byproducts. Gas products (N_2, H_2, and CO) were monitored using online gas chromatography. The concentration of produced NO_2^- was determined using the Griess method (Figs. S9 and S10 in Supporting information). As depicted in Fig. 3c, combined with Fig. 3b, at potentials below −0.5 V, the excess release of NH_3 and H_2 from intensified hydrogen evolution blocks the adsorption sites of CO_2 and NO_3^-. This impacts the urea electrosynthesis performance, leading to a diversified distribution of products, with NO_2^-, N_2, and CO also being detected. Enhanced hydrogen evolution significantly hinders the formation of C–N bonds by coupling *CO with $*NH_2$. The recyclability and stability of the electrocatalyst are crucial for industrial applications. Therefore, an 8-cycle electrosynthesis of urea was conducted, with results shown in Fig. S11 (Supporting information), Figs. 3d and e. The consistent current response, urea FEs, and yields indicate the durable stability of Mo_2C/C. Furthermore, a 12-h long-term electrolysis test at −0.5 V in CO_2-saturated 0.2 mol/L Na_2SO_4 containing 0.05 mol/L NO_3^- showed a steady current density, underlining the catalyst's potential for practical applications. The stability of Mo_2C/C during NO_3RR is further confirmed by a steady current density over 12 h of prolonged electrolysis (Fig. S12 in Supporting information). Additionally, post-electrolysis analysis shows nearly identical LSV curves (Fig. S13 in Supporting information), well-preserved morphology (Fig. S14 in Supporting information), and consistent XRD pattern (Fig. S15 in Supporting information), collectively demonstrating the high durability and stability of Mo_2C/C in this process.

To further reveal the underlying mechanism of urea electrosynthesis on 2D Mo_2C nanosheets from NO_3^- and CO_2, DFT computations were carried out. The atomic structure of Mo_2C is depicted in Fig. S16 (Supporting information). These calculations explored the entire free energy landscape of urea formation. The NO_3^- reduction follows a multi-step path-

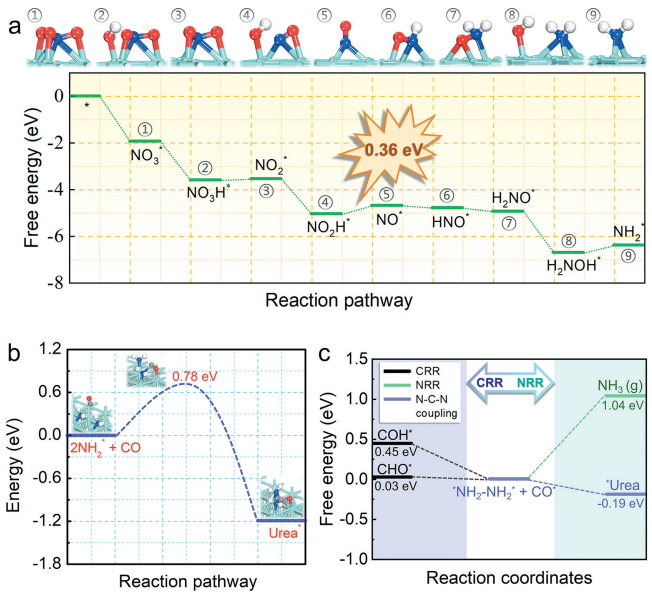

Fig. 4. (a) Free energy diagram and optimized geometrical structures of the involved reaction intermediates for NO_3^- reduction on Mo_2C. (b) The minimum energy pathway from (NH_2^* + NH_2^* + CO) to Urea* and the corresponding energy barrier. (c) The reaction energies in co-adsorbed $^*NH_2$–NH_2^* and CO further reaction.

way: $NO_3^- \rightarrow NO_3^* \rightarrow NO_2^* + OH^* \rightarrow NO_2^* \rightarrow NO^* + OH^* \rightarrow NO^* \rightarrow HNO^* \rightarrow H_2NO^* \rightarrow NH_2^* + OH^* \rightarrow NH_2^*$ [31]. Here, the formation of NO* represents the potential rate-limiting step, exhibiting a ΔG value of 0.36 eV (Fig. 4a). The presence of multiple Mo active sites significantly enhances the dissociation and hydrogenation of NO_3^*, NO_2^*, and H_2NO^* intermediates. The CO_2 reduction process follows the pathway $CO_2 \rightarrow COOH^* \rightarrow CO^*$, easily proceeding to *CO (Fig. S17 in Supporting information). Two mechanisms, Eley–Raideal and Langmuir-Hinshelwood, were then considered for the N–C-N coupling process. As depicted in Fig. 4b, the energy barrier for inserting CO between two independently adsorbed NH_2^* intermediates, leading to urea formation, is only 0.78 eV. This step is also thermodynamically favorable, with a ΔG value of –0.19 eV, indicating that CO and NH_2^* coupling is energetically advantageous both kinetically and thermodynamically. To assess Mo_2C nanosheet's selectivity for urea production, potential competitive reactions, such as NO_3^- reduction to NH_3, CO* hydrogenation, and the hydrogen evolution reaction (HER), were examined. The results revealed higher ΔG values for NH_2^* reduction to NH_3 and CO* hydrogenation (1.04 eV and 0.03 eV, respectively) compared to N–C-N coupling (–0.19 eV) (Fig. 4c), suggesting the thermodynamic unfeasibility of these reactions. For HER, its selectivity was evaluated by comparing the free energy change of H* adsorption with NO_3^- adsorption on Mo active sites. As shown in Fig. S18 (Supporting information), ΔG_{H^*} is –0.70 eV, more positive than $\Delta G_{NO_3^*}$, thus indicating a preference for NO_3^- reduction over HER. Consequently, the side reactions of NO_3^- reduction, CO* hydrogenation, and HER are substantially less favored compared to urea production, affirming the high selectivity of Mo_2C towards urea formation. *Ab initio* molecular dynamic (AIMD) simulations confirm that at 500 K, Mo_2C maintains its structure during 10 ps of annealing, with minimal fluctuations in total energy and temperature (Fig. S19 in Supporting information), further demonstrating Mo_2C's robust stability in urea formation.

In summary, we have successfully developed Mo_2C/C as a high-active catalyst for urea synthesis through the electrocatalytic coupling of NO_3^- and CO_2. The synthesized Mo_2C/C demonstrates exceptional catalytic efficiency, achieving a high urea production rate of 579.13 μg h^{-1} mg^{-1} and a FE of 44.80% at −0.5 V. Additionally, it exhibits remarkable electrochemical, maintaining its performance throughout 12 h of continuous electrolysis. Theoretical insights into the mechanism indicate that the formation of $^*NH_2$ and the retention of *CO on the Mo_2C's multiple active sites is crucial for facilitating C–N bond formation during urea electrosynthesis. This research not only showcases the potential of Mo_2C/C as an electrocatalyst for the ambient conversion of NO_3^- and CO_2 but also paves the way for future experimental and theoretical studies in developing 2D electrocatalysts with multiple active sites for sustainable production of organonitrogen compounds through C–N coupling.

Declaration of competing interest

The authors declare that they have no known competing financial interests or personal relationships that could have appeared to influence the work reported in this paper.

CRediT authorship contribution statement

Yue Zhang: Data curation, Writing – original draft. **Xiaoya Fan:** Data curation. **Xun He:** Data curation. **Tingyu Yan:** Formal analysis. **Yongchao Yao:** Formal analysis. **Dongdong Zheng:** Investigation. **Jingxiang Zhao:** Conceptualization, Writing – review & editing. **Qinghai Cai:** Investigation. **Qian Liu:** Validation. **Luming Li:** Validation. **Wei Chu:** Validation. **Shengjun Sun:** Validation. **Xuping Sun:** Conceptualization, Writing – review & editing.

Acknowledgment

The authors acknowledge support from the Natural Science Funds for Distinguished Young Scholar of Heilongjiang Province (No. JC2018004).

Supplementary materials

Supplementary material associated with this article can be found, in the online version, at doi:10.1016/j.cclet.2024.109806.

References

[1] S. Kim, S.H. Ye, A. Adamo, et al., J. Mater. Chem. B 8 (2020) 8305–8314.
[2] P.M. Glibert, J. Harrison, C. Heil, S. Seitzinger, Biogeochem 77 (2006) 441–463.
[3] A. Yapicioglu, I. Dincer, Renew. Sustain. Energy Rev. 103 (2019) 96–108.
[4] F. Barzagli, F. Mani, M. Peruzzini, Green Chem. 13 (2011) 1267–1274.
[5] J.G. Chen, R.M. Crooks, L.C. Seefeldt, et al., Science 360 (2018) 6391.
[6] S. Li, Y. Zou, C. Chen, S. Wang, Z.Q. Liu, Chin. Chem. Lett. 35 (2024) 109147.
[7] C. Chen, X. Zhu, X. Wen, et al., Nat. Chem. 12 (2020) 717–724.
[8] Y. Huang, Y. Wang, Y. Wu, et al., Sci. China Chem. 65 (2022) 204–206.
[9] X. Liu, Y. Jiao, Y. Zheng, et al., Nat. Commun. 13 (2022) 5471.
[10] Z. Zhang, D. Li, Y. Tu, et al., SusMat 4 (2024) e193.
[11] X. Fan, C. Liu, X. He, et al., Adv. Mater. (2024), https://doi.org/10.1002/adma.202401221.
[12] M. Yuan, J. Chen, Y. Bai, et al., Chem. Sci. 12 (2021) 6048–6058.
[13] X. Chen, S. Lv, J. Kang, et al., Proc. Natl. Acad. Sci. U. S. A. 120 (2023) e2306841120.
[14] M. Yuan, J. Chen, H. Zhang, et al., Energy Environ. Sci. 15 (2022) 2084–2095.
[15] X. Zhu, Y, Li, ACS Catal. 13 (2023) 15322–15330.
[16] J. Liu, X. Lv, Y. Ma, et al., ACS Nano 17 (2023) 25667–25678.
[17] J. Liang, Q. Liu, A.A. Alshehri, X. Sun, Nano Res. Energy 1 (2022) e9120010.
[18] H.Q. Yin, L.L. Yang, H. Sun, et al., Chin. Chem. Lett. 34 (2023) 107337.
[19] D. Chen, M. Luo, S. Ning, et al., Small 18 (2022) 2104043.
[20] D. Chen, J. Lan, F. Xie, et al., Chem. Eng. J. 475 (2023) 146137.
[21] J. Lan, M. Luo, J. Han, et al., Small 17 (2021) 2102814.
[22] W. Peng, M. Luo, X. Xu, et al., Adv. Energy Mater. 10 (2020) 2001364.
[23] X. He, J. Li, R. Li, et al., Inorg. Chem. 62 (2023) 25–29.
[24] J. Leverett, T. Tran-Phu, J.A. Yuwono, et al., Adv. Energy Mater. 12 (2022) 2201500.
[25] Y. Mao, Y. Jiang, H. Liu, et al., Chin. Chem. Lett. 35 (2024) 108540.
[26] Y. Luo, K. Xie, P. Ou, et al., Nat. Catal. 6 (2023) 939–948.
[27] X. He, T. Xie, K. Dong, et al., Sci. China Mater. (2024), doi:10.1007/s40843-024-2798-5.
[28] Y. Zhao, Y. Ding, W. Li, et al., Nat. Commun. 14 (2023) 4491.
[29] C. Chen, S. Li, X. Zhu, et al., Carbon Energy 5 (2023) e345.
[30] H. Song, D.A. Chipoco Haro, P.W. Huang, et al., Acc. Chem. Res. 56 (2023) 2944–2953.

[31] C. Tang, Y. Zheng, M. Jaroniec, S.Z. Qiao, Angew. Chem. Int. Ed. 133 (2021) 2–21.
[32] C. Lv, L. Zhong, C. Yan, et al., Nat. Sustain. 4 (2021) 868–876.
[33] Y. Mao, Y. Jiang, Q. Gou, et al., Appl. Catal. B: Environ. 340 (2024) 123189.
[34] Z. Li, P. Zhou, M. Zhou, et al., Appl. Catal. B: Environ. (338) (2023) 122962.
[35] J. Qin, N. Liu, L. Chen, et al., ACS Sustainable Chem. Eng. 10 (2022) 15869–15875.
[36] C. Liu, H. Tong, P. Wang, et al., Appl. Catal. B: Environ. 336 (2023) 122917.
[37] X. Zhu, X. Yuan, Y. Wang, M. Ge, Y. Tang, J. Catal. 429 (2024) 115218.
[38] Y. Wang, S. Xia, J. Zhang, et al., ACS Energy Lett. 8 (2023) 3373–3380.
[39] S. Shin, S. Sultan, Z.X. Chen, et al., Energy Environ. Sci. 16 (2023) 2003–2013.
[40] N. Meng, X. Ma, C. Wang, et al., ACS Nano 16 (2022) 9095–9104.
[41] F.Y. Chen, Z.Y. Wu, S. Gupta, et al., Nat. Nanotechnol. 17 (2022) 759–767.
[42] Y. Wang, W. Zhou, R. Jia, Y. Yu, B. Zhang, Angew. Chem. Int. Ed. 59 (2020) 5350–5354.
[43] J. Liang, Z. Li, L. Zhang, et al., Chem 9 (2023) 1768–1827.
[44] T. Zhao, K. Chen, X. Xu, et al., Appl. Catal. B: Environ. 339 (2023) 123156.
[45] R.D. Milton, S.D. Minteer, ChemPlusChem 82 (2017) 513–521.
[46] E. Murphy, Y. Liu, I. Matanovic, et al., ACS Catal. 12 (2022) 6651–6662.
[47] P. Huang, M. Cheng, H. Zhang, et al., Nano Energy 61 (2019) 428–434.
[48] M. Sun, G. Wu, J. Jiang, et al., Angew. Chem. Int. Ed. 62 (2023) e202301957.
[49] J. Yu, W. Yu, B. Chang, et al., Chin. Chem. Lett. 33 (2023) 3231–3235.
[50] Z. Nie, Z. Tang, D. Jiao, et al., ChemCatChem 14 (2022) e202101885.
[51] Y. Wu, K. Yao, Z. Zhao, et al., Chem. Eng. J. 479 (2024) 147602.
[52] X. Ye, J. Ma, W. Yu, et al., J. Energy Chem. 67 (2022) 184–192.
[53] N.H. Attanayake, H.R. Banjade, A.C. Thenuwara, et al., Chem. Commun. 57 (2021) 1675–1678.
[54] J. Li, C. Zhang, C. Wu, et al., Chin. Chem. Lett. 35 (2024) 108782.
[55] Y. Wan, M. Zheng, R. Lv, Mater. Today Energy 32 (2023) 101240.
[56] X. Ren, J. Zhao, Q. Wei, et al., ACS Cent. Sci. 5 (2019) 116–121.
[57] X. Liu, W. Sun, J. Chen, Z. Wen, Angew. Chem. Int. Ed. 136 (2023) e202317313.
[58] X. He, X. Li, X. Fan, et al., ACS Appl. Nano Mater. 5 (2022) 14246–14250.
[59] Z. Nie, L. Zhang, Q. Zhu, et al., J. Energy Chem. 88 (2024) 202–212.